UNIVERSITY OF CALIFORNIA, SAN DIEGO

The effects of abstinence from chronic ethanol administration on diffusion tensor imaging metrics and myelin-associated proteins in the medial prefrontal cortex

A Thesis submitted in partial satisfaction of the requirements

for the degree of Master of Science

in

Biology

by

Emmanuel Genaro Villalpando

Committee in charge:

Professor Chitra Mandyam, Chair
Professor Douglass Forbes, Co-Chair
Professor Steve Briggs

2017

The Thesis of Emmanuel Genaro Villalpando is approved and it is acceptable in quality and form for publication on microfilm and electronically:

Co-Chair

Chair

University of California, San Diego

2017

DEDICATION

I dedicate this thesis

to my parents, Genaro and Rosita,

and to my little sister, Hannah,

for their continued love and support.

EPIGRAPH

The man who does not read good books has no advantage over the man who cannot read them.

Mark Twain

TABLE OF CONTENTS

LIST OF FIGURES

ACKNOWLEDGEMENTS

I would first like to thank Dr. Chitra D. Mandyam for her unwaivering support, direction, and counsel during my time as a graduate student. Serving as both my principal investigator and the chair of my committee, her guidance has been invaluable throughout the course of my research efforts. In addition, I would like to thank Dr. Sucharita S. Somkuwar for her continued mentorship and help in all aspects of my work, as she continually strove to help me perform at my highest capacity and to strive for excellence in all that I did. Furthermore, I would like to give my thanks to our lab manager, McKenzie Fannon, for making all of our experiments possible through her expertise in running and managing our lab's experiments. This study was greatly supported through funding from the NIAAA and the NIH (AA020098 to CDM), without which none of this invaluable research experience would not have been possible for me.

ABSTRACT OF THE THESIS

The effects of abstinence from chronic ethanol administration on diffusion tensor imaging metrics and myelin-associated proteins in the medial prefrontal cortex

by

Emmanuel Genaro Villalpando

Master of Science in Biology

University of California, San Diego, 2017

Professor Chitra D. Mandyam, Chair
Professor Douglass Forbes, Co-Chair

Previous studies have shown that ethanol dependence induced by repeating cycles of chronic intermittent ethanol vapor exposure (CIE) followed by protracted abstinence (CIE-PA) produces significant alterations in gliogenesis in the rodent medial prefrontal

cortex (mPFC). Specifically, CIE-PA has been shown in previous studies to significantly dysregulate the process of myelinating oligodendrocytes in the mPFC by creating an unprecedented increase in premyelinating oligodendroglial progenitor cell (OPC) proliferation and survival, which has been associated with persistent elevated drinking behaviors during abstinence. In the current thesis, 63 male adult Wistar rats were subjected to seven weeks of CIE and were examined following 1 day(d), 7d, 21d, or 42d of abstinence. Neuroimaging, capable of detecting alterations to the myelination integrity of the mPFC *in vivo*, was performed in CIE-PA and age-matched non-vapor control rats, in parallel with conventional immunohistochemical methods to better characterize the physiological changes underlying any neuroimaging metric changes. This neuroimaging technique, called diffusion tensor imaging (DTI), successfully detected abstinence-related changes in the mPFC, specifically that CIE-PA produced transient increases in fractional anisotropy (FA) at the 7d abstinence time point compared to controls and other time points. Interestingly, this increase in FA, was associated temporally with increases in myelin basic protein (MBP), myelin oligodendrocyte glycoprotein (MOG), 2'3'-cyclic-nucleotide 3'-phosphodiesterase (CNPase) that we observed also occurred at the 7d PA time point. Therefore, this study concluded that DTI is capable of detecting myelination related changes in the mPFC that result from CIE-PA.

INTRODUCTION

Alcohol Use Disorder (AUD) currently afflicts over 15 million adults in the United States as of 2015, with the lifetime prevalence of adult Americans who have suffered from an AUD standing at a staggering 29.1% (Grant et al., 2017; SAMHSA et al., 2015). Of the current population of AUD individuals, less than 10% of them will receive treatment for their disorder, of which only 20-50% will achieve short-term remission (Cohen et al., 2007; Dawson et al., 2005). Furthermore, of the short-term remission achiever group, a significant proportion will fail to maintain abstinence, with the estimated long-term relapse rate for this population being as high as 80% (Finney et al., 1999; Moos et al., 2006). Hence, the need for the development of AUD treatments with greater short-term and long-term remission rates necessitates expanded study of the factors contributing to relapse vulnerability during the alcohol-abstinence process.

In order to effectively study AUDs, any animal model used to study alcohol dependence must encapsulate key dimensions of the disorder to provide data with sufficient external validity. Among these, an important criterion is that the model induces a withdrawal-like state that closely mirrors human withdrawal syndromes, as a result of ethanol usage cessation (McBride et al., 1998; Schulteis et al., 1996). For this reason, the use of chronic intermittent ethanol (CIE) vapor exposure protocols have grown in prominence as a way to better study the underlying neuropathology that is the resultant of chronic alcohol usage. This well-established technique involves inducing ethanol dependence via continued cycles of a continuous ethanol vapor exposure period followed by a forced abstinence period for a prolonged duration of time (Gilpin et al., 2008). This strategy has been shown to successfully induce ethanol dependence in rodents, as

assessed by the resultant somatic and motivational symptoms achieved during forced withdrawal, including voluntary escalation in ethanol drinking, persistent anxiety-like behavior, and dysregulation of reward thresholds (Becker et al., 2013; Griffin et al., 2009; Griffin et al., 2014; Lopez et al., 2005; Lopez 2012).

The rodent medial prefrontal cortex (mPFC) is a region that has been shown to be significantly affected as a result of the CIE paradigm (Mandyam et al., 2012). The region is a functional homolog of the human prefrontal cortex, which is involved in a multitude of higher order functioning processes involving the formation of behavior-action functional associations, social cognition, and self-regulation through behavioral inhibition (Bicks et al., 2015; Euston et al., 2012; Moorman et al., 2015; Preston et al., 2013; Weilbacher et al., 2016). Hence, the prefrontal cortex acts as a fundamental component of the neural circuits of self-control that are dysregulated in those with substance addiction disorders such as AUDs (Abernathy et al., 2010). This highlights the significant importance of understanding why the human frontal cortex region is especially vulnerable to alcohol's neurodegenerative effects on myelination, and consequently, white matter integrity. The nature of these deleterious alterations has been characterized by post-mortem studies, which have shown a significant decline in glial cell density, levels of myelin-related transcripts, and myelin-related protein expression in the superior frontal cortex region of human alcohol-dependent individuals (Lewohl et al., 2000; Lewohl et al., 2005; Mayfield et al., 2002; Miguel-Hidalgo et al., 2006). These changes in turn indicate that it is the oligodendrogenesis role of the mPFC that should be of key interest in understanding the mechanism of alcohol-related white matter neuropathology. Under normal conditions, the adult mammalian mPFC is a proliferative site of self-

renewing glial progenitors, with the majority of such progenitors maturing into neuron-glial antigen 2 (NG2+) oligodendrocyte progenitor cells (NG2-OPCs) and subsequently, myelinating oligodendrocytes (OLGs) (Somkuwar et al., 2014; Mandyam et al., 2007). However, this process has been shown to be significantly altered as a result of CIE in a way with significant implications (Kim et al., 2015; Navarro et al., 2015; Richardson et al, 2009; Somkuwar et al., 2015).

For example, previous studies from our lab have shown that chronic ethanol exposure via CIE and forced protracted abstinence, which is defined as abstinence for greater than 24hr, from CIE (CIE-PA) induce significant and seemingly opposite patterns of dysregulation of myelinating oligodendrogenesis in the mPFC. Specifically, this region in CIE animals exhibited a decrease in the capacity of glial progenitors to proliferate and differentiate into premyelinating OLGs, a decrease in the resident population of premyelinating OLGs, and a corresponding decrease in expression of proteins associated with myelination (Kim et al., 2015; Richardson et al., 2009; Mandyam et al., 2012). Furthermore, CIE was determined to block the maturation of pre-myelinating OLGs into myelinating OLGs in a manner dependent on the hyperphosphorylation of the basic helix-loop-helix transcription factor Olig2 (Kim et al., 2015; Sun et al., 2011). Acute withdrawal from CIE has also been shown in Samantaray et al., 2015, to significantly downregulate CNS expression of key myelin-associated proteins in a manner associated with axonal degeneration, indicating that the effects of deficits in myelinating OLGs translate into the disruption of myelin integrity. In contrast, CIE-PA has been shown to induce a spike in OPC proliferation at the 72h withdrawal time point, of which a significant proportion of OPCs survive 28d post-CIE cessation and manifests as an

elevation in levels of pre-myelinating and myelinating OLG markers in the mPFC (Somkuwar et al., 2015). CIE-PA has been shown to significantly upregulate myelin-associated protein expression, which in conjunction with its induction of the hypophosphorylation of Olig2, suggests that CIE-PA is promoting maturation of premyelinating OLGs into myelinating OLGs (Navarro et al., 2015; Somkuwar et al., 2016). Furthermore, the presence of these alterations to oligodendrogenesis and cortical myelination, occurring in tandem with a persistent elevation in ethanol drinking and anxiety-like behavior during abstinence, suggests the presence of compensatory mechanisms that may contribute to relapsing propensity through the dysregulation of the mPFC glial cell niche (Pleil et al., 2015; Van Skike et al., 2015; Valdez et al., 2002).

Diffusion tensor imaging (DTI) is a novel, non-invasive neuroimaging method that is used to detect alterations in axonal integrity and myelination that conventional structural magnetic resonance imaging (MRI) is incapable of measuring (O'Donnell et al., 2011, Soares et al., 2017). For this reason, our lab decided to use this technique as a way to further investigate and characterize alterations in the myelination of the mPFC as a consequence of the CIE-PA paradigm. DTI involves generating image contrast based on differences in the directionality, magnitude, and freedom of movement of water molecule diffusion in different tissues on a per-voxel basis, with a voxel being a unit of volumetric space in computer-based modeling (Alexander et al., 2007). Important DTI metrics calculated for each voxel are mean diffusivity (MD), which describes the average magnitude of diffusion occurring independent of directionality, and fractional anisotropy (FA), which is a measure of the degree of directional selectivity of diffusion. An FA value can range from 0 to 1 on a normalized scale, with a score of 0 entailing that

diffusion is isotropic, or of equal magnitude in all directions, while a score of 1 indicates that diffusion is fully anisotropic, or completely predominant along a single axis. Regions in which diffusion is highly restricted along certain axes, such as the white matter tracts of the corpus callosum, tend to have higher FA values, while regions such as the ventricles, which are membranous sacs filled with cerebrospinal fluid (CSF), have FA values near zero (Chanraud et al., 2010). Hence, the technique is able to detect alterations in the cellular composition, organization, and microstructure of tissue regions because changes to such aspects of tissue will affect diffusion (Alexander et al., 2007; Soares et al., 2017). Specifically, in relation to white matter, FA values serve as measures of white matter axonal tract integrity and thus the extent of axonal myelination, while MD values are regarded as indexes of the extent of fluid invasion into tracts (Basser et al, 1996; Pierpaoli et al., 2001; Pfefferbaum et al., 2005; Rosenbloom et al., 2003).

Numerous DTI studies have indicated that alcoholism results in differential disruption of the white matter integrity of frontal white matter tract projections to cerebellar, limbic, occipital, and parietal regions. These studies emphasize that the pattern of white matter disruption in frontal cortex regions that occurs as the result of chronic ethanol usage in AUD individuals, has been consistently characterized as significantly lowered FA values and elevated MD levels, (Fortier et al., 2014; Konrad et al., 2014; Pfefferbaum et al., 2000; Pfefferbaum et al., 2014; Sorg et al., 2012; Zahr et al., 2017). In turn, such a pattern of changes has been associated with decreased tract coherence, involving disruptive changes to axon morphology, compromised myelin integrity, and edema of extracellular fluid in surrounding tissues (Pfefferbaum et al., 2005). Furthermore, the detrimental cognitive effects resulting from such damage to frontal

cortex regions have been consistently shown to be associated with specific deficits in psychomotor processing speed, visuospatial memory, and working memory (Harper et al., 2007; Pfefferbaum et al., 2005; Pfefferbaum et al., 2006; Rosenbloom et al., 2003, Rosenbloom et al., 2008). Hence this pattern of lowered FA and elevated MD can be said to be a clinically relevant marker of alcohol-related neuropsychological damage. However, prolonged abstinence from alcohol exhibits therapeutic effects in that it has been shown to result in recovery from frontal region FA deficits, in conjunction with decreases in elevated MD values, in the timespan of weeks to months (Alhassoon et al., 2012; Chaunraud et al., 2009; Gadzkinski et al., 2010; Zou et al., 2017). Perhaps most intriguing, in terms of characterizing the relationship between changes in DTI metrics and relapsing behavior, is a study (Sorg et al. 2012) revealing significantly lower FA in the frontal lobe of AUD individuals that relapse to heavy-drinking post-treatment in comparison to those that maintained abstinence or drank at minimal levels. Furthermore, a trajectory of FA increase in frontal white matter tracts and, hence, restoration of fiber integrity, has been shown to occur in alcoholics who remained abstinent after treatment, while alcoholics who relapsed expressed a trajectory of FA decrease (Pfefferbaum et al., 2014).

Although it is tempting to infer that this recovery of FA values in frontal-cortical regions corresponds with certain physiological changes resulting in the non-relapsing phenotype, it must be recognized that to fully characterize the mechanism of recovery of microstructural white matter integrity detected via DTI, conventional forms of tissue analysis must be utilized. Hence the present need to substantiate the correlative relationship of specific DTI measures with particular microstructural aberrations has

renewed emphasis towards the use of animal models in the study of alcohol use disorders (De la Monte et al., 2014; Oguz et al., 2015; Zahr et al., 2017). In support of this notion, multiple studies have shown that unique DTI metric expression patterns are consistently and reliably able to detect changes in myelination status, axonal integrity, inflammatory lesions, and the location of such pathology in particular white matter tracts, as confirmed through the use of supporting protein, histological, morphological, and genomic analysis. (Song et al., 2002; Song et al., 2005; Deboy et al., 2007; Mac Donald et al., 2007; Kim et al., 2005; Wu et al., 2008; Zhang et al., 2012).

Given the capacity of small animal DTI to be used in conjunction with biochemical methods, this experiment was designed to allow for the physiological characterization and verification of any detectable changes in white matter integrity occurring in the rodent mPFC as a result of CIE-PA. Following *in vivo* DTI scanning at either the 1d, 7d, 21d, or 42d abstinence time points selected during CIE-PA, immediate animal sacrifice allowed for cortical tissue collection and subsequent analysis. Having multiple points during CIE-PA analyzed allowed for an assessment of time-dependent changes in the DTI metrics of FA and MD, that were then explained more mechanistically utilizing Western blot analysis of myelin-associated proteins and glial cell populations within the mPFC. The primary hypothesis of this experiment was that DTI would detect changes in FA and MD values in the rodent mPFC at different time points during the abstinence period of CIE-PA. The secondary hypothesis was that such observed changes in FA and MD value would be correlated with the elevated expression of myelin-associated proteins and myelinating oligodendrogenesis in the mPFC that has been observed as a consequence of CIE-PA.

MATERIALS AND METHODS

Animals

Sixty-three adult male Wistar rats (Charles River, Hollister, CA USA), aged 8-weeks old and weighing between 275-325g at the start of the experiment, completed this study. Animals were housed in a temperature-controlled (22˚C) vivarium with ad libitum access to food and water. Animals were set on a 12-hour (hr) light/ 12hr dark cycle, with the light cycle beginning at 8:00PM, in groups of 2 to 3 animals per cage unit. All experimental protocols used in this study were approved by The Scripps Research Institute and the VA San Diego Healthcare System Institutional Animal Care and Use Committee and were performed in accordance with the National Institutes of Health Guide for the Care and Use of Laboratory Animals (NIH Publication No. 85–23, revised 1996).

Chronic intermittent ethanol vapor exposure and protracted abstinence (CIE-PA)

During this experiment, animals were randomly assigned to either CIE-PA or non-CIE-PA (age-matched non-vapor controls) group. CIE-PA rats were exposed to cycles of ethanol vapor produced via vaporization of 95% ethanol in a heated flask that was immediately conveyed through controlled air flow to rat vapor chambers on a 14-h on/ 10-h off daily schedule for the duration of seven weeks. The vapor flow rate was calibrated so as to achieve animal target blood alcohol levels within the range of 125 to 250 mg/dL (27.2 to 54.4 mM), which has been shown to induce voluntary escalation in drinking behavior, in addition to both physical dependence and negative behavioral affect during ethanol withdrawal (Gilpin 2008, Griffin 2009a, Griffin 2009b, Griffin 2014, Lopez 2005). Following seven weeks of cyclic vapor exposure, CIE-PA animals

underwent protracted abstinence from ethanol exposure. CIE-PA animals were then randomly assigned into four separate CIE-PA time-point groups that were subjected to either 1d (n=10), 7d (n=9), 21d (n=9), or 42d (n=9) of forced abstinence, at which point they underwent structural and DTI scanning, and were then immediately sacrificed while still completely anesthetized (**Figure 1**). Age-matched non-vapor controls for 1d (n=8), 7d (n=6), 21d (n=6), or 42d (n=6) CIE-PA animals were scanned and sacrificed on the same day as their respective vapor-exposed group.

Blood alcohol levels (BALs) measurements

In order to assess animal BALs and ensure that they were within the designated target range, blood samples (0.2mL) from CIE-PA animals were collected immediately post-daily vapor exposure via tail-bleeding. Samples were collected twice during the first week of exposure, and weekly for the subsequent six weeks. After collection, the samples were centrifuged, and isolated plasma aliquots (5μL) were assessed utilizing an Analox AM1 analyzer (Analox Instruments USA Inc., MA, USA) to determine BALs. For each set of samples, the reagents provided by Analox Instruments (25–400 mg/dL or 5.4–87.0 mM) were utilized to perform the necessary single-point calibrations. Ethanol vapor levels were adjusted accordingly when animal BALs fell outside of the target range of 125-250 mg/dL. Mean BALs of CIE-PA animals throughout the course of the seven weeks of vapor exposure were then determined (**Figure 2**).

Magnetic resonance imaging (MRI)

Conventional T2-weighted MRI and DTI were performed on all rats at the assigned time point post-cessation of seven weeks of CIE for CIE-PA animals, and their respective age-matched non-vapor controls. These scan sessions occurred at 1d post-

ethanol cessation or post-natal day (PND) 105, 7d or PND 126, 21d or PND126, and 42d or PND147. All imaging was performed on a Bruker 7 Tesla/20cm horizontal bore small animal MRI system (Bruker BioSpec, Ettingen, Germany), with use of bite bar to affix rat head in standardized prone position for all subjects in order to minimize motion artifacts. This was done after the initiation of subject anesthetization with a 3.0 volume % isoflurane and 1.2-1.4 l/min oxygen flow mixture, which was delivered to each subject via nose cone for duration of scan. After head placement, a two-channel local receive radiofrequency (RF) coil was fitted over head and secured into place using tape to further reduce possible motion disturbances due to breathing. Vitals were continuously monitored throughout duration of the scan session via usage of a respiratory monitor to detect breathing rate and a rectal probe to monitor core temperature, which was kept at approximately 37˚C through the use of a continuous flow of heated air.

All imaging sessions began with use of a standard localizer scan (TriPilot) to position the subject head in optimal orientation for coronal plane slice acquisition. Following this, anatomical and T2-weighted imaging protocols were executed for each animal scan, prior to running a standard DTI protocol. The T2-weighted images were acquired using a fast spin echo (FSE) imaging sequence protocol: TR= 8308.7ms, TE= 36.0ms, flip angle = 180.0˚, NEX= 6, slices per subject = 60, slices with slice thickness =400µm, acquisition matrix =256 x 128, field of view=20.5mm x 20.5mm, in-plane resolution= 80 µm x 160µm, and time = 13 m 17 s per individual. Diffusion tensor imaging was performed using a 30 direction, multi-shot spin echo planar-imaging sequence (DTI-EPI) protocol utilizing diffusion-weighted gradients with b-value = 1000 s/mm^2 applied in six noncollinear directions, with an additional five b= 0 s/mm^2 images

collected. This DTI-EPI protocol has been utilized in similar DTI addiction studies of the rodent brain performed on a 7T scanner (McKenna et al., 2016). The scanning parameters for DTI were as follows: TR = 7500.0ms, TE= 23.4ms, flip angle= 90.0˚, NEX= 1, slices per subject = 30, slice thickness = 600µm, acquisition matrix = 176 x 80, field of view=28.2mm x 12.8mm, in-plane resolution=160µm x 160µm, and time = 8m 0s per individual. All DTI scans were followed by a conventional DTI TOPUP Distortion Correction protocol in order to correct for common geometric distortions that are the resultants of magnetic field susceptibility effects that occur during echo-planar DTI image acquisition (Andersson et al., 2003).

DTI image processing

Samples of regions of interests in grey and white matter were manually selected over DTI images utilizing Bruker Paravision Software Version 5.1 software at five distinct rat neuroanatomical regions of interest (ROIs), which were the infralimbic cortex, prelimbic cortex, anterior cingulate cortex, motor cortex (MC), and corpus callosum(CC). It should be noted that the infralimbic, prelimbic, and anterior cingulate cortices constitute regions of the mPFC, and all data from them was averaged to give a combined mPFC value for each DTI metric measured. The Paravision Software was first used to calculate the diffusion tensors and subsequently used for determination of DTI metrics for the defined ROIs. This was done utilizing the software's image reconstruction program, which performed the complete reconstruction of all DTI image slices, generating standard eigenvalue and eigenvector maps for every image slice within every series of DTI images collected for each animal. Subsequently, Paravision-generated maps of FA and trace values were generated. The five ROIs of interest were then located and

manually selected through consistent referral to drawing rules defining the maximum boundaries of each ROI as determined utilizing Paxinos et al., 2009 atlas reference. These five ROIs were each selected over each hemisphere, resulting in a total of ten ROIs placed over a single slice, one for each aforementioned brain region per hemisphere. For each subject, one 600μM slice was selected and slice selection was limited to scan slice sections located between bregma 3.72mm to 3.00mm, in the coronal plane, which encompasses a minimal boundary approximation of the rat medial prefrontal cortex. This was done in order to ensure that calculated metrics for each selected ROI were limited to and specified to those regions, such that measurements from adjacent neuroanatomical structures would not influence DTI metrics determined. By doing such, partial voluming effects (the contamination of an ROI with data from other regions) were minimized. Subsequently, FA and trace values within the selected regions were automatically calculated by the Paravision software statistical analysis program, and subsequently recorded. Trace values were then converted to MD values using the appropriate calculations.

T2-Image volumetric image processing

To assess the effect of ethanol withdrawal on the size of the rodent mPFC, defined structurally as the combined infralimbic, prelimbic, and anterior cingulate cortices, the image analysis and 3D visualization software Amira was used in the volumetric analysis of the T2-images of all animals (n=63). Previous structural MRI studies on human AUD patient brains have consistently shown persistent volumetric shrinkage effects in frontal cortical regions even after limited recovery due to periods of prolonged abstinence (Bae et al., 2016; Cardenas et al., 2007; Fortier et al., 2011;

Pfefferbaum et al. 2014; Zahr et al., 2017). For this reason, we sought to assess any possible volumetric changes in the mPFC region as a result of the CIE-PA protocol. Using Amira, manual segmentation of the mPFC was then performed on selected slices using a landmark-based strategy in which neuroanatomical regions with sharp contrast boundaries were used as reference points to delineate anatomical structures (Cox et al., 2014; Crespo-Facorro et al., 1999; McCormick et al., 2006; Wolf et al., 2002). Per subject two 400μM slices were selected, with slice selection limited to the range of bregma 3.72mm to 3.00mm, in the coronal plane. This encompassed a minimal boundary approximation of the rat medial prefrontal cortex in the coronal plane that was established using Paxinos et al., 2009 as an atlas reference (**Figure 8c**).

The mPFC was outlined by beginning at the point of the corpus callosum that was most ventromedial, which was approximately 1mm from the coronal plane midline. From this point, a line was drawn directly downwards for 0.5 mm, after which a connecting line was made directly perpendicular from this point, such that it went directly medial and connected with the coronal midline. From this point, a line was drawn directly vertical until the most dorsal point of the coronal axis midline was reached. Returning to the most ventral point of the corpus callosum, the curvature of the medial boundary of the corpus callosum was then traced until the most dorsomedial point on the corpus callosum was reached. Next, beginning at the most dorsal point on the midline of the coronal axis, an approximately 0.5mm line was drawn laterally at a 45degree angle to the horizontal axis, from which the most dorsal point on the midline was upon. Finally, a line was drawn from this point, back to the most dorsomedial point of the corpus callosum. After this, the AMIRA software's autofill feature was utilized to fill in the unselected region outlined by

the manual tracing. This process was repeated twice for each slice, one time for each hemisphere. The AMIRA software used for 3D reconstruction of manually segmented mPFC portion selected within this range and subsequent volumetric calculation and determination was performed by software to generate volumetric data.

Western blot analysis

Optimized western blot protocols were utilized in order to measure levels of myelin-associated proteins and total proteins at each time point during the abstinence period of the CIE-PA protocol (Kim et al., 2015; Somkuwar et al., 2014; Somkuwar et al., 2015). Immediately after scanning sessions were completed, rapid decapitation of isoflurane anesthetized CIE-PA (n= 37) and age-matched non-vapor control (n=26) animals were performed. After rapid removal, brains were cut along the mid-sagittal axis, with 4% paraformaldehyde utilized to fixate the right hemisphere, while the left hemisphere was flash frozen for tissue-punching. Subsequently, 500µm slices from the mPFC were cut, from which tissue punches were collected, homogenized via sonication using ice-cold buffer (320 mM sucrose, 5 mM HEPES, 1 mM EGTA, 1 mM EDTA, 1% SDS, with Protease Inhibitor Cocktail and Phosphatase Inhibitor Cocktails II and III diluted 1:100; Sigma, St. Louis, MO), and heated for a period of five minutes at 100˚C. All samples were subsequently stored at a temperature of -80˚C until protein concentration was determined through the use of a detergent-compatible Lowry method (Bio-Rad, Hercules, CA), before being mixed (1:1) with Laemmli sample buffer containing β-mercaptoethanol. Following this, 20µg aliquots of each sample were ran on 8-12% SDS-PAGE gel, prior to being transferred to PVDF membranes (0.2µm pore size).

After transfer, 5% milk (w/v) in TBST solution (25 mM Tris-HCl (pH 7.4), 150 mM NaCl and 0.1% Tween 20 (v/v)) was used to block all blots at 4˚C for 16 to 20hr. Blots were then incubated in at 4˚C for 16-20h in primary antibody: antibody to cyclic nucleotide phosphodiesterase (CNPase) (1:2000, Cell Signaling cat. 5664, predicted band size 47kDa, observed band ~47 kDa), antibody to myelin oligodendrocyte glycoprotein (MOG) (1:1000, Thermo Fischer Scientific cat. pa5-19602, predicted molecular weight 25 kDa, observed band ~25kDa), antibody to myelin basic protein (MBP) (1:500, Abcam, cat. no. ab40390, predicted band size 18–23 kDa, observed band ~20 kDa), antibody to oligodendrocyte lineage transcription factor 2 (Olig2) (1:10000, generous gift from Drs. Charles Stiles and John Alberta, Harvard University, predicted molecular weight 37 kDa (Ligon et al., 2006), observed band ~37 kDa), antibody to phosphorylated-oligodendrocyte lineage transcription factor 2 (pOlig2) Ser-10, 13,14 (1:500, generous gift from Drs. Charles Stiles and John Alberta, Harvard University, predicted molecular weight 35 kDa, observed band ~35 kDa (Sun et al., 2011)). As a loading control, β-tubulin (1:8,000, Santa cruz cat. no. sc-5274, predicted band size 50 kDa, observed band ~50 kDa) was utilized. The blots were then washed for three cycles over 15 minutes in TBST, from which they were subjected to a 1h, room temperature (24˚C) incubation in either horseradish peroxide–conjugated goat antibody to rabbit (1:10,000, BioRad) or horseradish peroxide–conjugated goat antibody to mouse IgG1 (1:10,000, BioRad) in TBST. An additional washing period of three cycles over 15 minutes in TBST was then performed before immunoreactivity detection, using SuperSignal West Dura chemiluminescence detection reagent (Thermo Scientific) and collection using HyBlot CL Autoradiography film (Denville Scientific) and a Kodak film processor. The software

Image J (version 1.45S, NIH) was then utilized to determine net intensity values from blots. Subsequently, blots were stripped for 20 minutes at room temperature (Restore, Thermo Scientific). After stripping, blots were reprobed for β-Tubulin (1:8000, SCBT sc-53140) for normalization purposes. In order to make value comparisons between groups, unpaired Student's t tests were used.

Statistical Analysis

The effect of duration of CIE-PA on fractional anisotropy, mean diffusivity, and myelin-associated protein levels were analyzed using one-factor ANOVA, followed by post-hoc analysis using Tukey's and Dunnett's post hoc tests. Unpaired Student's t-test were utilized to assess the effect of group (control vs CIE-PA) on fractional anisotropy, mean diffusivity, and myelin-associated protein levels. Data are expressed as mean ± SEM and statistical significance for values was set at $p<0.05$. All analysis performed on GraphPad Prizm software.

RESULTS

CIE produces elevated and consistent blood alcohol levels

The experimenter-adjusted BALs of the CIE-PA animals took two weeks to acclimate to the target BAL range of 125 and 250 mg/dl (**Figure 2**). After reaching this range at week 3, BALs remained within target range for the remaining duration of the CIE treatment period, for a total of five weeks.

In controls, no changes were observed in fractional anisotropy (FA) values of the mPFC, motor cortex, and corpus callosum

In order to control for possible confounding effects on observing a true effect of duration of abstinence on FA values in the mPFC, the FA values of our ROIs in controls was assessed. Analysis of the FA values in age-matched non-vapor controls for each respective CIE-PA group showed no significant differences between these control groups in terms of FA values in the mPFC [$F(3, 22) = 1.032$, $p=0.3976$], motor cortex [$F(3, 22) = 2.024$, $p=0.1399$], and corpus callosum [$F(3, 22) = 1.748$, $p=0.1865$], regions (**Figure 3**).

CIE-PA transiently elevates FA Values in the mPFC at the 7d abstinence time point

Fractional anisotropy values in the mPFC for each CIE-PA group were expressed as percentages of each group's respective age-matched vapor controls (**Figure 4a**). Analysis of differences between the different durations of abstinence for each CIE-PA group revealed that the effect of duration of CIE-PA on FA value in the mPFC was significant [$F(3, 33) = 4.174$, $p<0.05$]. Post-hoc analysis showed a significant difference between the FA values of the 7d and 42d CIE-PA groups ($p<0.01$), with an approximate

15.56 % decrease in FA at the 42d CIE-PA group relative to the 7d CIE-PA group. Separate T-tests for individual time points revealed a transient elevation in FA value of the mPFC in the 7d abstinence CIE-PA group relative to age-matched non-vapor controls ($p=0.0186$).

Aging has no effect on MD values in the mPFC, motor cortex, and corpus callosum

In order to control for possible confounding effects on observing a true effect of duration of abstinence on MD values in the mPFC, the MD values of our ROIs in controls was assessed was assessed. Analysis of the FA values in age-matched non-vapor controls for each respective CIE-PA group showed no significant differences between these control groups in terms of MD values in the mPFC [$F(3, 22) = 2.458$, $p=0.0897$], motor cortex [$F(3, 22) =1.051$, $p=0.3899$], and corpus callosum [$F(3, 22) =2.685$, $p=0.0715$] regions (**Figure 5**).

Duration of abstinence in CIE-PA affects MD Values in the mPFC

Mean Diffusivity values in the mPFC for each CIE-PA group were expressed as percentages of each group's respective age-matched vapor controls (**Figure 6a**). Analysis of differences between the different durations of abstinence for each CIE-PA group revealed that the duration of abstinence on MD value in the mPFC was significant [$F(3, 33) = 4.871$, $p < 0.01$], indicating that another mPFC DTI metric exhibited a duration-of-withdrawal dependent effect. Further analysis showed a small, but significant difference between the MD values in the mPFC of the 1d and 42d CIE-PA groups ($p = 0.0259$), with an approximate 5.55% lower MD value in the 1d CIE-PA group relative to the 42d CIE-

PA group. Additionally, another small, but significant difference between the MD values of the 21d and 42d CIE-PA groups ($p = 0.0124$) was found, with an approximate 6.26% lower MD value in the 21d CIE-PA group relative to the 42d CIE-PA group.

Duration of abstinence in CIE-PA affects MD Values in the motor cortex

Mean Diffusivity values in the motor cortex for each CIE-PA group were expressed as percentages of each group's respective age-matched vapor controls (**Figure 6b**). Analysis of differences between the different durations of abstinence for each CIE-PA group revealed that the effect of duration of CIE-PA on MD value in the motor cortex was significant [$F(3, 33) = 5.768$, $p<0.005$]. Post-hoc analysis showed a significant difference between the MD values of the 1d and 7d CIE-PA groups ($p = 0.0185$), with an approximate 15.22% lower MD value in the 1d CIE-PA group relative to the 7d CIE-PA group. Additionally, another significant difference between the MD values of the 1d and 42d CIE-PA groups ($p = 0.0025$) was found, with an approximate 18.92% lower MD value in the 1d CIE-PA group relative to the 42d CIE-PA group.

The volume of the mPFC is not affected by the duration of abstinence in CIE-PA nor in controls

In order to ensure that volumetric effects would not confound DTI metric values, volumetric measurements of the mPFC were taken for all animals (**Figure 8a-b**). Analysis showed no difference in volume of the mPFC the age-matched non-vapor controls for each respective CIE-PA group [$F= (3, 23) = 0.1685$, $p=0.9165$]. Additional

analysis showed that the different durations of abstinence for each CIE-PA group also had no effect on the volume of the mPFC [F= (3, 35) = 0.0394, p=0.9894].

CIE-PA transiently elevates levels of CNPase expression in the mPFC at the 7d abstinence time point

To investigate the effects of different durations of abstinence in CIE-PA on CNPase expression in the mPFC, Western blot analysis was conducted (**Figure 9a, c**). Analysis of differences between the different durations of abstinence for each CIE-PA group revealed that the duration of abstinence had a significant effect on CNPase expression in the mPFC [F(4,57) = 3.638, p = 0.0104]. Post-hoc analysis showed a transient elevation in CNPase expression of the mPFC in the 7d abstinence CIE-PA group relative to controls (p=0.0067). As a late-stage oligodendrocyte lineage marker, elevations in CNPase levels indicates enhanced OPC maturation into immature and myelinating oligodendrocytes (Barateiro et al., 2014). This marker was utilized in conjunction with assessment of myelin-associated proteins in order to elucidate if increases in myelin were associated with increases in total OLG population.

CIE-PA transiently elevates levels of MBP expression in the mPFC at the 7d abstinence time point

To investigate the effects of different durations of CIE-PA on MBP expression in the mPFC, Western blot analysis was conducted. Analysis of differences between the different durations of abstinence for each CIE-PA group revealed that the effect of duration of CIE-PA on MBP expression was significant in the mPFC [F(4,57) = 3.639, p

= 0.0430]. Post-hoc analysis showed a transient elevation in MBP expression of the mPFC in the 7d abstinence CIE-PA group relative to controls (**Figure 9a-b**, p=0.0025). This result is consistent with previous studies utilizing the same CIE-PA paradigm, which showed elevated MBP levels during CIE-PA (Kim et al., 2015; Navarro et al., 2015).

CIE-PA transiently elevates levels of MOG expression in the mPFC at the 7d time point

To investigate the effects of different durations of CIE-PA on MOG expression, Western blot analysis was conducted (**Figure 9a, e**). Analysis of differences between the different durations of abstinence for each CIE-PA group revealed that the effect of duration of CIE-PA on MOG expression was significant in the mPFC [$F(4,57) = 3.157$, $p = 0.0206$]. Post-hoc analysis showed a transient elevation in MBP expression of the mPFC in the 7d abstinence CIE-PA group relative to controls (p=0.0280). The dysregulation of expression levels of MOG, another myelin-associated protein in addition to MBP, substantiates a narrative of myelination abnormalities in the mPFC as a consequence of CIE-PA.

CIE-PA trends towards a transient depression in levels of pOlig2 expression in the mPFC at the 21d time point

To investigate the effects of different durations of CIE-PA on pOlig2 expression, Western blot analysis was conducted (**Figure 9b, f**). Individual pOlig2 expression values were calculated as a percentage of total Olig2 (tOlig2) for each rat, such that the pOlig2 value is calculated as a ratio of pOlig2 to tOlig2. Analysis of differences between the

different durations of abstinence for each CIE-PA group revealed that the effect of duration of CIE-PA on pOlig2 expression in the mPFC, trended towards a decrease in pOlig2 levels, although this effect did not reach significance [$F(4,57) = 2.481$, $p=0.0562$]. This trend is in agreement with results from a previous study from our lab, that showed that CIE-PA induces hypophosphorylation of Olig2 (and hence a decrease in pOlig2 levels), in a manner that was associated with elevation in MBP levels (Navarro et al., 2015). Literature has shown that hypophosphorylation of Olig2 is associated with increased maturation of immature oligodendrocytes into mature myelinating oligodendrocytes, which would corroborate with elevated expression of myelin-associated proteins, such as MOG (Sun et al., 2011).

DISCUSSION

The primary goal of my thesis was to determine whether withdrawal from chronic ethanol usage, as established through the protracted abstinence in the CIE-PA protocol, would produce time-dependent changes in FA and MD values in the mPFC, as detected through the use of *in vivo* DTI. The secondary goal was to determine whether any detected changes in DTI metrics would be associated with elevations in myelin-associated protein expression and myelinating oligodendrogenesis. Although previous studies have demonstrated that CIE-PA significantly alters the process of myelinating oligodendrogenesis in the mPFC (Navarro et al., 2015; Richardson et al., 2009; Somkuwar et al., 2015; Somkuwar et al., 2016) the use of DTI to characterize such changes in this gray matter region is a novel application of this neuroimaging technique. Furthermore, this study provided a more comprehensive analysis of the protracted abstinence portion of CIE-PA, by assessing neuroimaging metrics and supporting protein data at a multitude of time points: the 1d, 7d, 21d, and 42d into abstinence.

Although it was found that the length of abstinence in CIE-PA had significant effects on MD values in the mPFC and MC regions, the biological significance of such effects are unknown. This is because the magnitude of the observed differences between the MD values of the differing CIE-PA groups in these two regions were small and did not differ significantly from controls. Further studies should look at the effect of varying lengths of abstinence from chronic ethanol usage on MD values in frontal brain regions, because elevated diffusivity values are a sign of alcohol-related pathological accumulation of fluid and disruption of microstructure (Mori et al., 2006). However, it was demonstrated that duration of abstinence in CIE-PA produced a significant, transient

increase in FA in the mPFC at the 7d abstinence time point. This showed that DTI could be used to detect changes induced by abstinence from chronic ethanol usage in the mPFC region. Furthermore, because the MD and FA values in the mPFC, motor cortex, and corpus callosum did not significantly differ between the age-matched non-vapor controls for each respective CIE-PA group, this detected change in FA could be interpreted as a true effect of the CIE-PA protocol. Given that FA is a measure of the amount of diffusion occurring along directionally-specific orientation, higher FA values are generally a baseline characteristic of regions of the brain that contain highly organized and directed diffusion, namely the highly myelinated axons of white matter fiber tracts connecting regions such as the prefrontal cortex to other key neural structures (Arfanakis et al., 2002; Bihan et al., 2003; Chanraud et al., 2010; Soares et al., 2013). Furthermore, this high FA value has been established as a correlate of healthy white matter fiber integrity, and studies on recovering alcoholics have found that the first few weeks to months of the sustained abstinence period is characterized by significant recovery from consistently observed decreases in FA that were present during chronic ethanol usage (Alhassoon et al., 2012; Gadzinski et al., 2010; Pfefferbaum et al., 2014; Zahr et al., 2017). Thus, increases in FA are generally associated with abstinence-related recovery through increased axon integrity, of which a major component of maintaining is the extent of myelination (Rosenbloom et al., 2008; Zahr et al., 2008).

In addition to the observed increase in FA value, it was found that CIE-PA produced a significant increase in the expression of MBP, MOG, and CNPase, all myelin-associated proteins and markers of myelinating oligodendrocytes, that also occurred in the mPFC at the same 7d abstinence time point as the observed FA increase. A trending

towards significant transient decrease in pOlig2 expression was also found at the 21d CIE-PA abstinence time point. Given that a decrease in pOlig2 has been correlated with enhanced maturation of OPCs into myelinating oligodendrocytes (Sun et al., 2011), this result supported findings from a previous study (Navarro et al., 2015) that CIE-PA induces hypophosphorylation of pOlig2 and hence enhanced maturation of OPCs into myelinating oligodendrocytes. For these reasons, the observed elevation in FA in the mPFC was interpreted as a consequence of an overexpression of myelination, and hence density of myelinating oligodendrocytes beyond normal levels of myelin expression. Further support for this notion came from the finding that CIE-PA had no effect on the volume of the mPFC, indicating that any decreases in myelination would be due to a decrease in levels of total myelin density, and not due to a structural volumetric shrinkage phenomena.

One possible explanation for this elevation in myelination observed at the 7d protracted abstinence time point is based on the observation from previous studies (Kim et al., 2016; Somkuwar et al., 2015) that CIE-PA induces enhanced OPC proliferation at the 72hr abstinence time point, from which there is an increase in survival and differentiation of these OPCs into myelinating oligodendrocytes (Cui et al., 2015). This enhanced differentiation response and consequent increase in myelination levels of the mPFC could be a product of an elevated neuroinflammatory response, which itself has been a well-established resultant of prolonged abstinence from chronic ethanol usage (Crews et al., 2012; Crews et al., 2015; Montesinos et al., 2016). Several studies have pointed to the essential role that neuroinflammatory factors such as tumor necrosis factor α (TNFα), in the process of OPC-dependent remyelination from experimentally induced

demyelination (Arnett et al., 2001; Bieber et al., 2004; Kotter et al., 2001; Waly et al., 2014). In fact, in Foote et al., 2005, it was demonstrated that in a rodent model of multiple sclerosis, transplanted OPCs required the stimulation of an inflammatory response in order to engage in the remyelination of a chronically demyelinated region. In further support of the neuroimmune-oligodendrogenesis connection, a recent publication (Somkuwar et al., 2016) has demonstrated that CIE-PA induces elevated levels PECAM-1, important mediator of dynamic regulation of blood-brain barrier integrity in response to neuroinflammation (Cheung et al., 2015; Privratsky et al., 2014; Woodfin et al., 2007), has that was shown to be associated with increased proliferation and survival of OPCs in the mPFC. Hence, the observed transient increase ins FA in the mPFC could be a product of an increase in myelinating oligodendrogenesis caused by a neuroimmune response catalyzed by protracted abstinence from ethanol during CIE-PA. In addition, it should be noted the CIE-PA has been shown to consistently produce elevated drinking levels during abstinence in rodents (Gilpin et al., 2008; Griffin et al., 2014), a behavior that has important clinical relevance to relapsing behavior in abstinent alcoholics. Altogether, these findings suggest that future research should further characterize the behavioral implications of both CIE-PA-induced dysregulation of myelinating oligodendrogenesis and blocking such dysregulation, in order to further assess the effect that the phenomena has on drinking behavior. In addition, later studies should continue to explore the use of DTI as an effective, non-invasive method for characterizing myelination integrity changes of the mPFC, given that this study has shown the technique's capacity to assess such alterations. Thus, continued translational efforts to establish the relationship between patterns of change as detected by DTI and conventional tissue analysis methods

should be made. This is because the use of DTI as a potentially clinically-efficient way to monitor the effectiveness of existing and potential pharmaceutical and behavioral therapies for recovering alcoholics presents a possible mechanism for better assessing and adjusting treatment strategy for those suffering from alcohol use disorders.

FIGURES

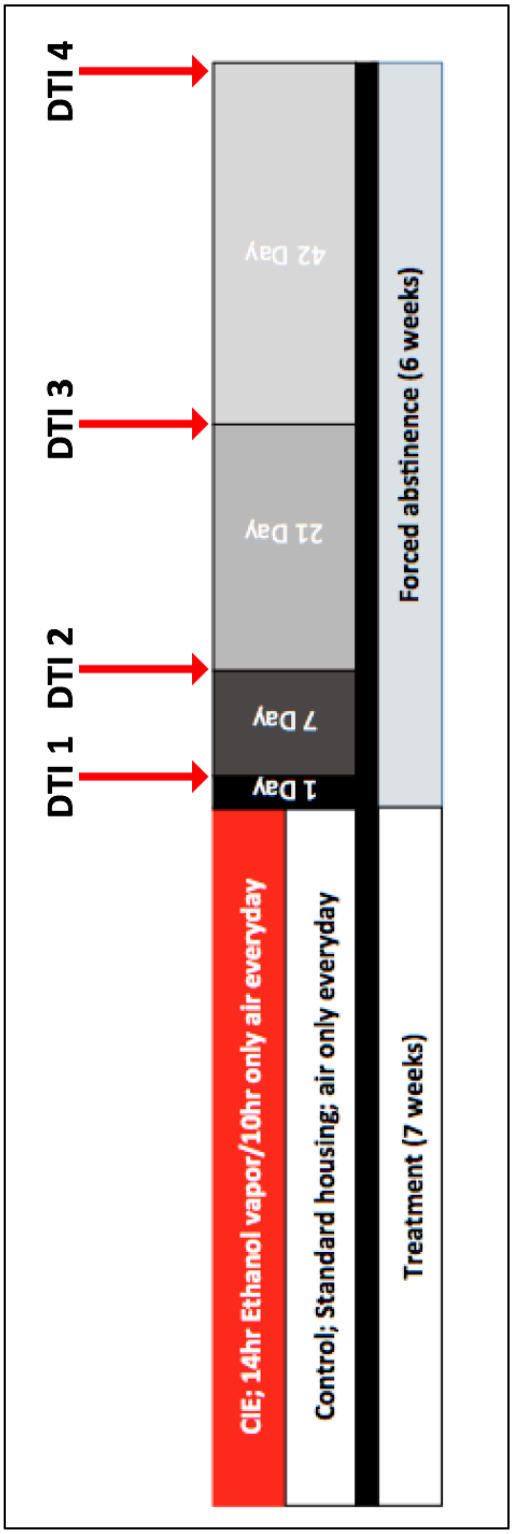

Figure 1: Schematic detailing experimental design and layout. A total of 63 adult male Wistar rats completed this experiment. Thirty-seven of these animals underwent seven weeks of CIE exposure as a part of the CIE-PA protocol, before being subjected to either 1d, 7d, 21d, or 42d of abstinence. Twenty-six served as age-matched non-vapor controls, and did not experience CIE exposure. CIE-PA animals from each of the four abstinence groups, and their respective age-matched non-vapor controls. All animals were scanned while anesthetized with 3.0 vol% isoflurane, and immediately sacrificed post-scanning.

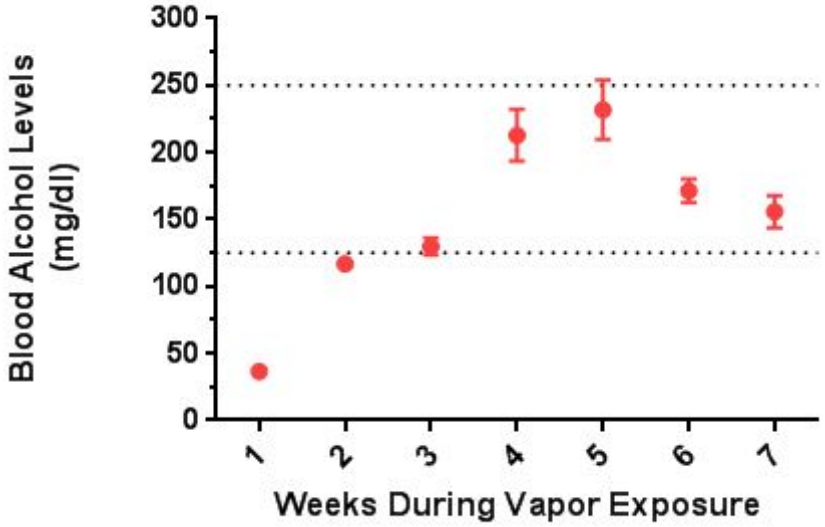

Figure 2: **Stable blood alcohol levels are produced by chronic intermittent ethanol vapor exposure.** Mean blood alcohol levels (BALs) in mg/dl for CIE-PA animals over the course of the seven weeks of CIE prior to PA period. The lower and upper bounds of dotted lines indicate, respectively, the 125 mg/dl and 250 mg/dl target BAL interval limits.

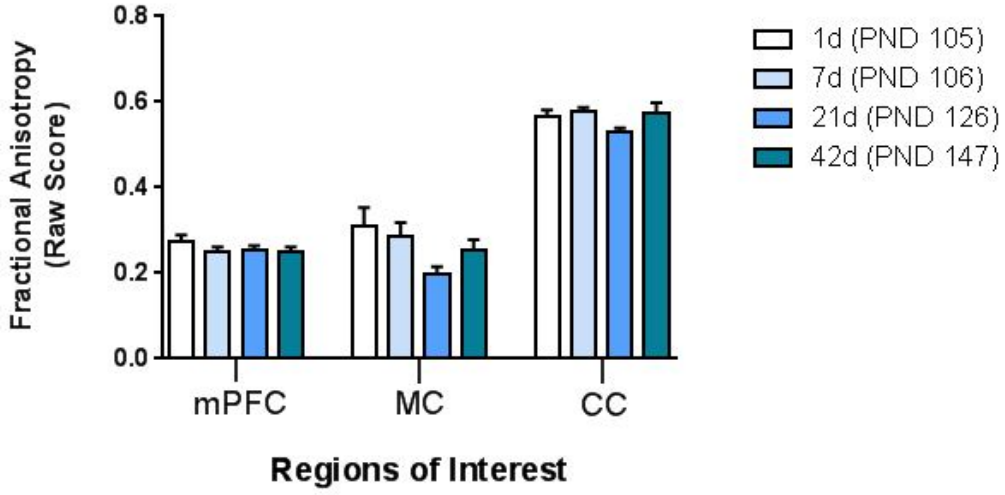

Figure 3: **Fractional anisotropy scores in the mPFC, motor cortex, and corpus callosum are unchanged in controls.** Raw fractional anisotropy (FA) scores for age-matched non-vapor controls in the medial prefrontal cortex (mPFC), motor cortex (MC), and corpus callosum (CC) regions are shown. Legend indicates postnatal day(PND) age of rats in each control group. No significant changes in raw FA values were detected in any region between the age-matched non-vapor controls for each respective CIE-PA group. n = 8 for 1d age-matched non-vapor control animals, n = 6 for 7d age-matched non-vapor control animals, n = 6 for 21d age-matched non-vapor control animals, and n = 6 for 42d age-matched non-vapor control animals.

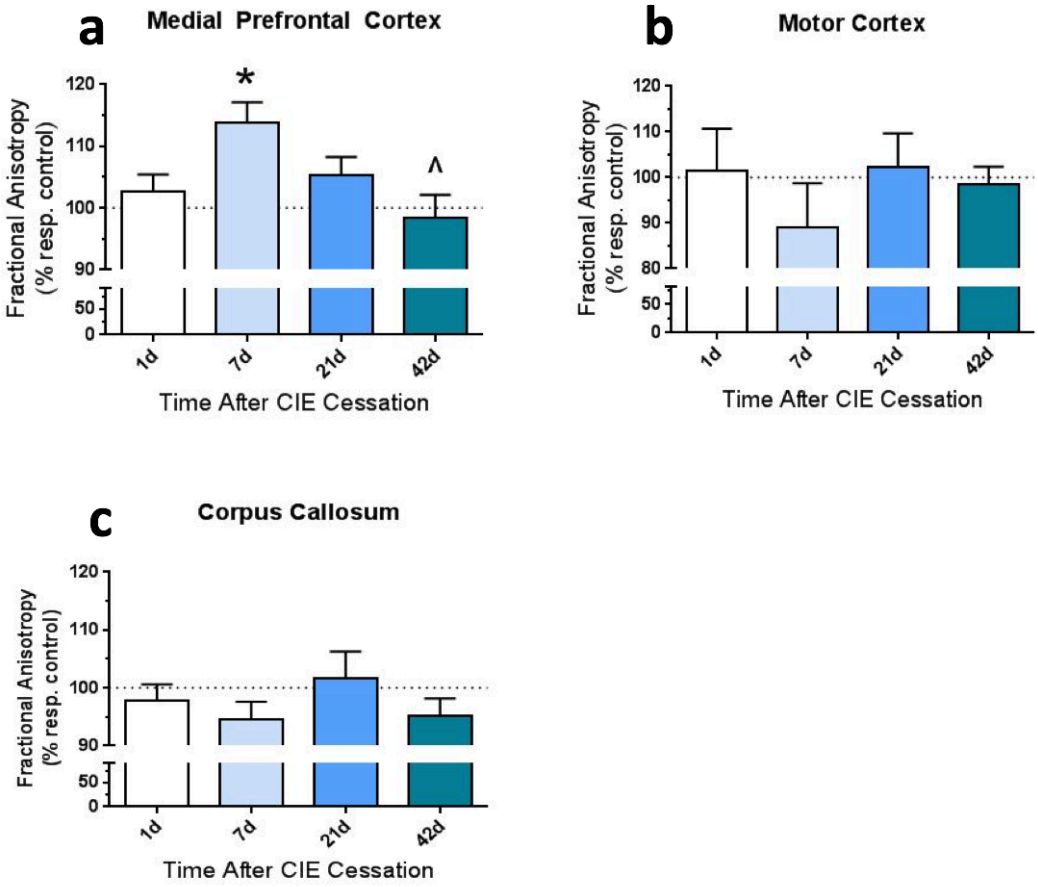

Figure 4: CIE-PA increases fractional anisotropy in the mPFC at the 7d abstinence time point. (a) CIE-PA increases fractional anisotropy in the mPFC at the 7d protracted abstinence time point. Analysis of fractional anisotropy values in the (a) mPFC, (b) MC, and (c) CC of 1d, 7d, 21d, and 42d CIE-PA animals expressed as percent change compared with controls. $n = 10$ for 1d CIE-PA animals, $n = 9$ for 7d CIE-PA animals, $n = 9$ for 21d CIE-PA animals, and $n = 9$ for 42d CIE-PA animals. *$p<0.05$ compared with controls, "^"$p<0.05$ compared with 1d CIE-PA group.

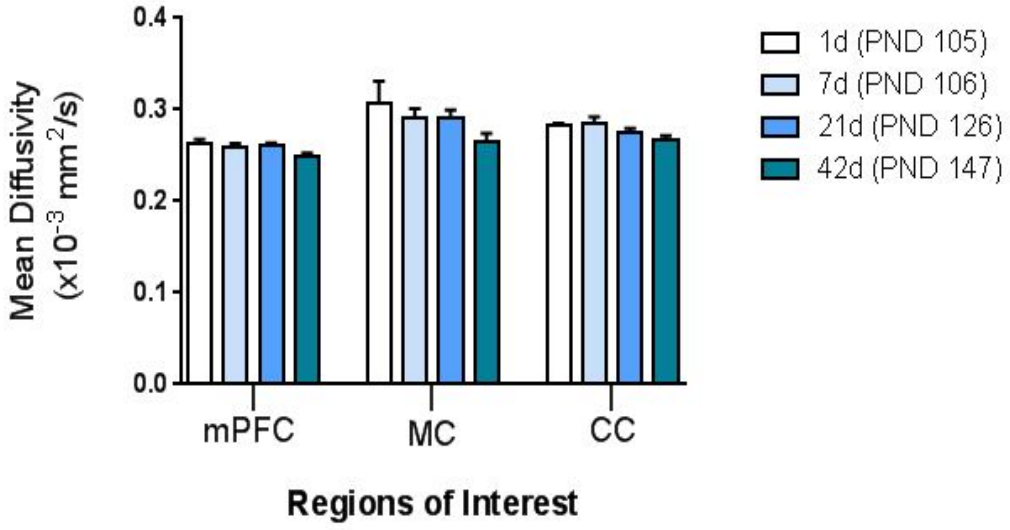

Figure 5: **Mean diffusivity values in the mPFC, motor cortex, and corpus callosum are unchanged in controls.** Raw mean diffusivity (MD) scores for age-matched non-vapor controls in the medial prefrontal (mPFC), motor cortex (MC), and corpus callosum (CC) regions are shown. Legend indicates postnatal day(PND) age of rats in each control group. No significant changes in raw MD values were detected in any region between the age-matched non-vapor controls for each respective CIE-PA group. $n = 8$ for 1d age-matched non-vapor control animals, $n = 6$ for 7d age-matched non-vapor control animals, $n = 6$ for 21d age-matched non-vapor control animals, and $n = 6$ for 42d age-matched non-vapor control animals.

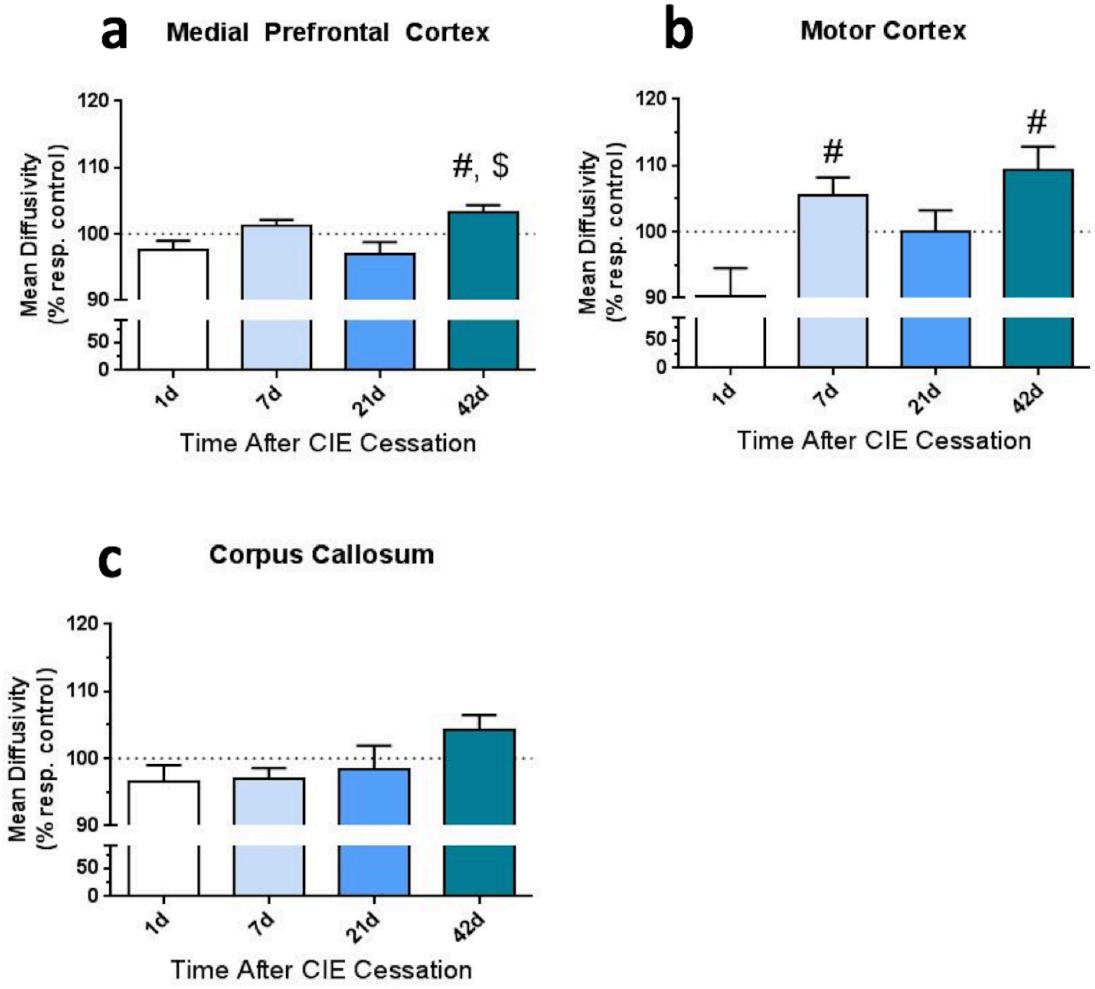

Figure 6: **CIE-PA affects mean diffusivity values in the mPFC and the motor cortex.** Analysis of mean diffusivity values in the (a) mPFC, (b) MC, and (c) CC of 1d, 7d, 21d, and 42d CIE-PA animals expressed as percent change compared with controls. *n* = 10 for 1d CIE-PA animals, *n* = 9 for 7d CIE-PA animals, *n* = 9 for 21d CIE-PA animals, and *n* = for 42d CIE-PA animals. *p<0.05 compared with controls, "#"p<0.05 compared with 1d CIE-PA group, "$"p<0.05 compared with 21d CIE-PA group.

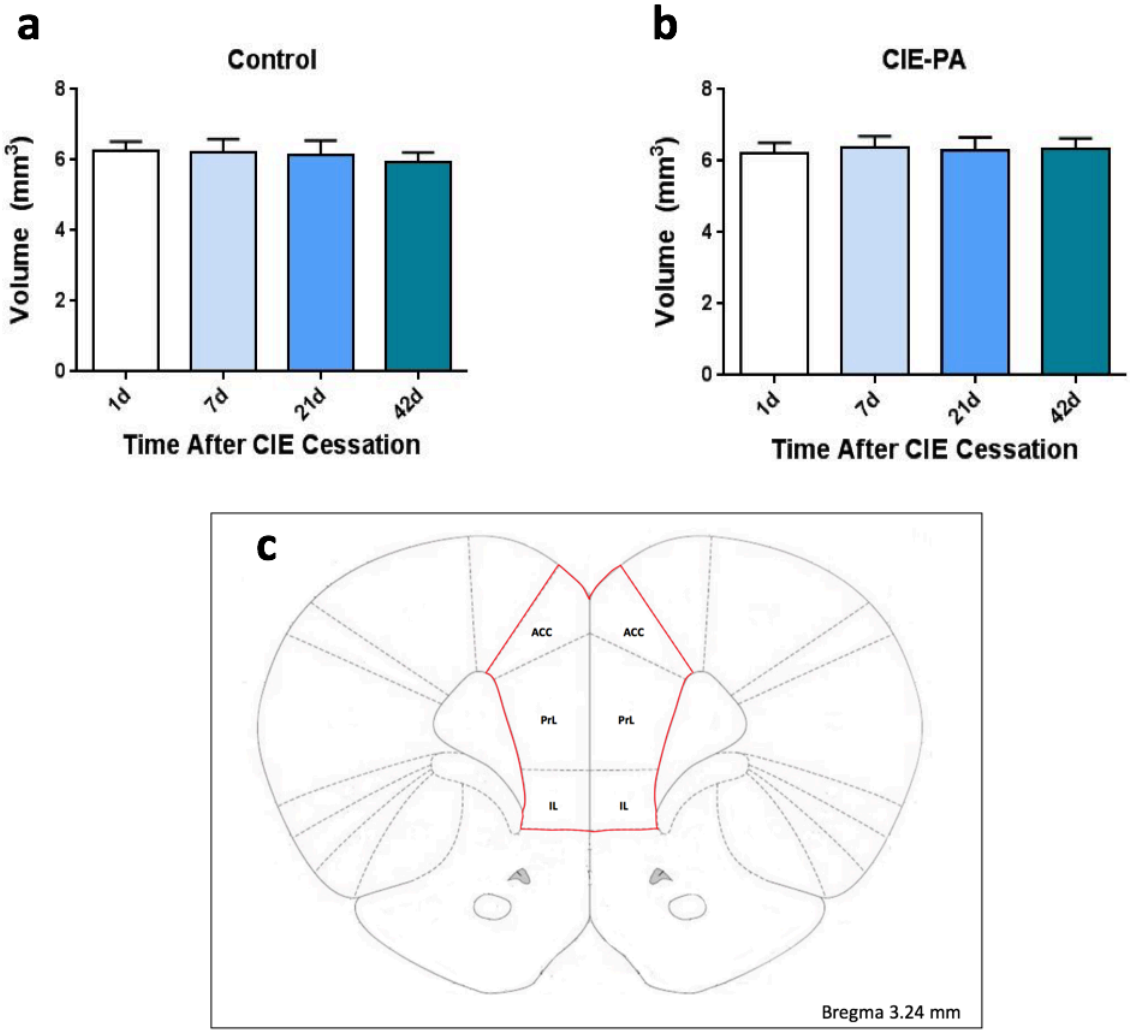

Figure 7: The volume of the mPFC is not affected by CIE-PA. Neither (a) the age-matched non-vapor controls for each respective CIE-PA group nor (b) the CIE-PA groups experienced a significant change in the volume of the mPFC. A representative atlas image (c) adapted from Paxinos et al., 2009, depicting the boundary of the mPFC, composed of the infralimbic (IL), prelimbic (PrL), and anterior cingulate cortices (ACC), outlined in red. n = 10 for 1d CIE-PA animals, n = 9 for 7d CIE-PA animals, n = 9 for 21d CIE-PA animals, and n = for 42d CIE-PA animals. n = 8 for 1d age-matched non-vapor control animals, n = 6 for 7d age-matched non-vapor control animals, n = 6 for 21d age-matched non-vapor control animals, and n = 6 for 42d age-matched non-vapor control animals.

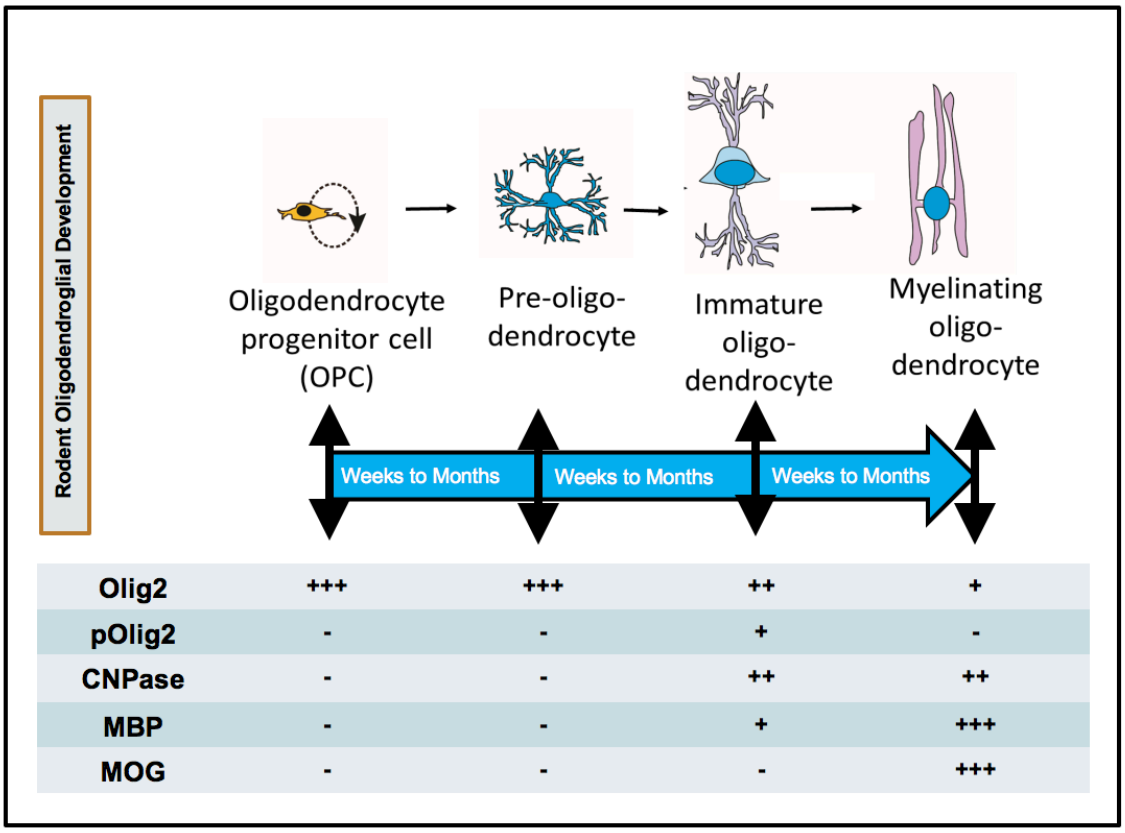

Olig2	+++	+++	++	+
pOlig2	-	-	+	-
CNPase	-	-	++	++
MBP	-	-	+	+++
MOG	-	-	-	+++

Figure 8: **Schematic detailing oligodendrocyte lineage maturation stages and corresponding relative expression of certain protein markers.** Schematic depicting the relative expression of Olig2, pOlig2 (phosphorylated Olig2), CNPase, MBP, and MOG, at each of the oligodendrocyte development stages. "-" indicates not present, "+" indicates present at comparatively low levels, ""++" indicates present at comparatively moderate levels, and "+++" indicates present at comparatively high levels relative to expression at the other stages of the oligodendrocyte lineage. Diagram adapted from Somkuwar et al., 2014.

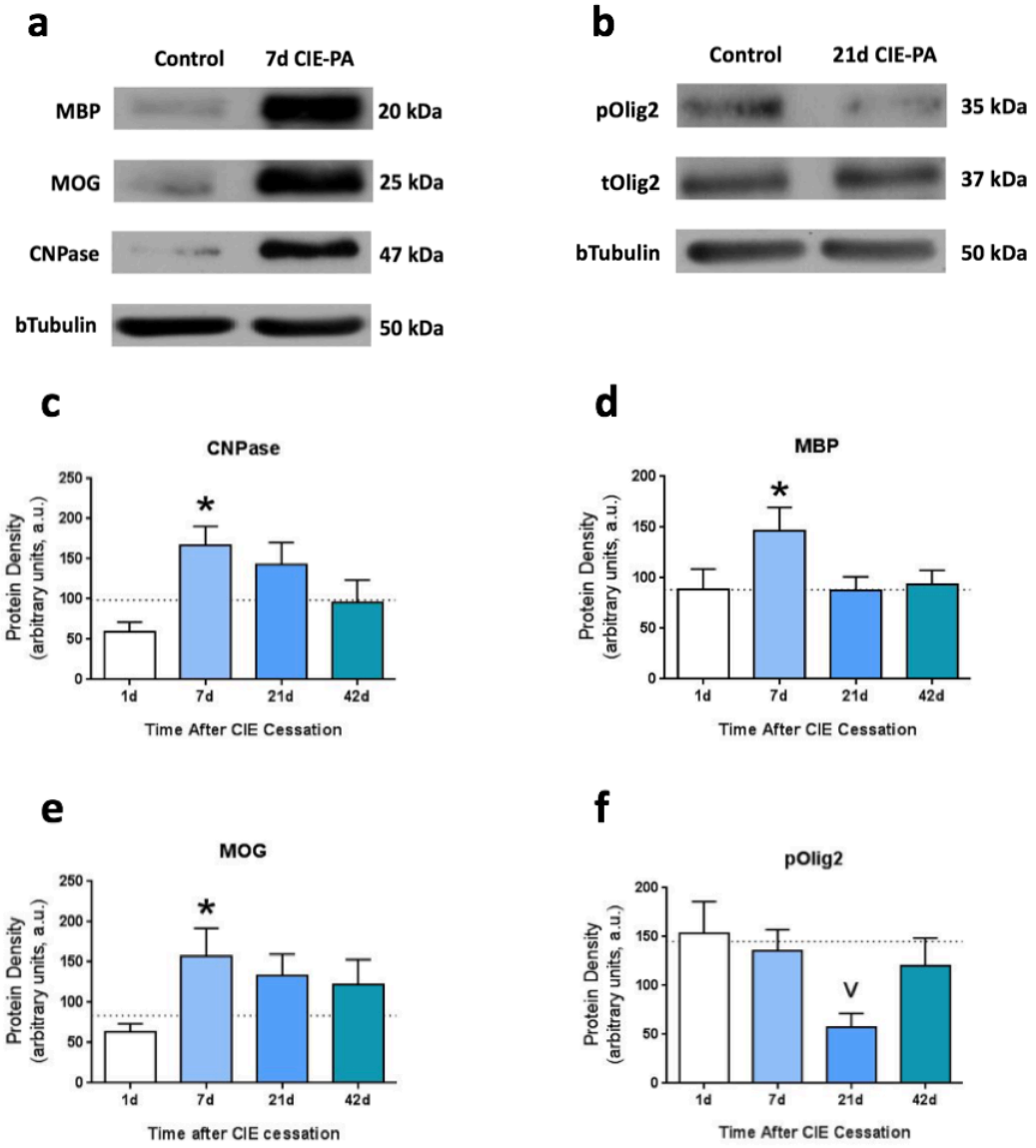

Figure 9: CIE-PA increases expression of myelin-associated proteins and markers of late-stage oligodendroglial lineage cells. CIE-PA increases the expression of late-stage oligodendroglial lineage markers and myelin-associated proteins in the mPFC at the 7d abstinence time point. (a) Representative immunoblots of CNPase, MBP, and MOG expression in controls versus 7d CIE-PA animals. (b) Representative immunoblots of pOlig2 and tOlig2 expression in controls versus 7d abstinence CIE-PA animals. (b-f) Analysis of protein densities in CIE-PA animals expressed as percent respective controls. Dotted line indicates controls' average. n = 10 for 1d CIE-PA animals, n = 9 for 7d CIE-PA animals, n = 9 for 21d CIE-PA animals, and n = for 42d CIE-PA animals. n = 8 for 1d age-matched non-vapor control animals, n=6 for 7d age-matched non-vapor control animals, n = 6 for 21d age-matched non-vapor control animals, and n = 6 for 42d age-matched non-vapor control animals. *$p<0.05$ compared with controls, "v"$p=0.05$ compared with controls.

REFERENCES

Alexander AL, Lee JE, Lazar M, Field AS. Diffusion tensor imaging of the brain. Neurotherapeutics. 2007;4(3):316-29.

Alhassoon OM, Sorg SF, Taylor MJ, Stephan RA, Schweinsburg BC, Stricker NH, Gongvatana A, Grant I. Callosal white matter microstructural recovery in abstinent alcoholics: a longitudinal diffusion tensor imaging study. Alcohol Clin Exp Res. 2012;36(11):1922-31.

Andersson JL, Skare S, Ashburner J. How to correct susceptibility distortions in spin-echo echo-planar images: application to diffusion tensor imaging. Neuroimage. 2003;20(2): 870-88

Bae S, Kang I, Lee BC, Jeon Y, Cho HB, Yoon S, Lim SM, Kim J, Lyoo IK, Kim JE, Choi IG. Prefrontal Cortical Thickness Deficit in Detoxified Alcohol-dependent Patients. Exp Neurobiol. 2016;25(6):333-341.

Basser J, Pierpaoli C. Microstructural and physiological features of tissues elucidated by quantitative diffusion tensor MRI. J Magn Reson 1996; 111: 209–219.

Becker HC. Animal models of excessive alcohol consumption in rodents. Current Topics in Behavioral Neurosciences. 2013;13:355–377.

Bicks LK, Koike H, Akbarian S, Morishita H. Prefrontal Cortex and Social Cognition in Mouse and Man. Front Psychol. 2015;6:1805.

Blanco AM, Guerri C. Ethanol intake enhances inflammatory mediators in brain: role of glial cells and TLR4/IL-1RI receptors. Front Biosci. 2007; 12:2616 –2630.

Blanco AM, Valles SL, Pascual M, Guerri C. Involvement of TLR4/ type I IL-1 receptor signaling in the induction of inflammatory mediators and cell death induced by ethanol in cultured astrocytes. J Immunol. 2005; 175:6893– 6899.

Cardenas VA, Studholme C, Gazdzinski S, Durazzo TC, Meyerhoff DJ. Deformation-based morphometry of brain changes in alcohol dependence and abstinence. Neuroimage. 2007;34(3):879-87.

Chanraud S, Zahr N, Sullivan EV, Pfefferbaum A. MR diffusion tensor imaging: a window into white matter integrity of the working brain. Neuropsychol Rev. 2010;20(2):209-25.

Cheung K, Ma L, Wang G, Coe D, Ferro R, Falasca M, Buckley CD, Mauro C, Marelli-Berg FM. CD31 signals confer immune privilege to the vascular endothelium. Proc Natl Acad Sci USA. 2015;112(43):E5815-24.

Cohen E, Feinn R, Arias A, Kranzler HR. Alcohol treatment utilization: Findings from the National Epidemiologic Survey on Alcohol and Related Conditions. Drug and Alcohol Dependence. 2007;86:214–221.

Cox SR, Ferguson KJ, Royle NA, Shenkin SD, MacPherson SE, MacLullich AM, Deary IJ, Wardlaw JM. A systematic review of brain frontal lobe parcellation techniques in magnetic resonance imaging. Brain Struct Funct. 2014;219(1):1-22.

Crespo-Facorro B, Kim JJ, Andreasen NC, O'Leary DS, Wiser AK, Bailey JM, Harris G, Magnotta VA. Human frontal cortex: an MRI-based parcellation method. Neuroimage. 1999;10(5):500-19.

Crews, F.T. Immune function genes, genetics, and the neurobiology of addiction. Alcohol Research: Current Reviews. 2012; 34(3):355–361.

Crews FT, Sarkar DK, Qin L, Zou J, Boyadjieva N, Vetreno RP. Neuroimmune Function and the Consequences of Alcohol Exposure. Alcohol Res. 2015;37(2):331-41, 344-51.

Cui C, Noronha A, Warren KR, Koob GF, Sinha R, Thakkar M, Matochik J, Crews FT, Chandler LJ, Pfefferbaum A, Becker HC, Lovinger D, Everitt BJ, Egli M, Mandyam CD, Fein G, Potenza MN, Harris RA, Grant KA, Roberto M, Meyerhoff DJ, Sullivan EV. Brain pathways to recovery from alcohol dependence. Alcohol. 2015;49(5):435-52.

Dawson DA, Grant BF, Stinson FS, Chou PS, Huang B, Ruan WJ. Recovery from DSM-IV alcohol dependence: United States, 2001–2002. Addiction. 2005;100(3):281–292.

Deboy CA, Zhang J, Dike S, Shats I, Jones M, Reich DS, Mori S, Nguyen T, Rothstein B, Miller RH, Griffin JT, Kerr DA, Calabresi PA. High resolution diffusion tensor imaging of axonal damage in focal inflammatory and demyelinating lesions in rat spinal cord. Brain. 2007;130(Pt 8):2199-210.

De la Monte SM, Kril JJ. Human alcohol-related neuropathology. Acta Neuropathol. 2014;127(1):71-90.

Euston DR, Gruber AJ, Mcnaughton BL. The role of medial prefrontal cortex in memory and decision making. Neuron. 2012;76(6):1057-70.

Finney JW, Moos RH, Timko C. The course of treated and untreated substance use disorders: remission and resolution, relapse and mortality. In: McCrady, B.; Epstein, E., editors. Addictions: a comprehensive guidebook. New York: Oxford University Press. 1999. p. 30-49.

Foote AK, Blakemore WF. Inflammation stimulates remyelination in areas of chronic demyelination. Brain. 2005;128(Pt 3):528-39.

Fortier CB, Leritz EC, Salat DH, Venne JR, Maksimovskiy AL, Williams V, Milberg WP, McGlinchey RE. Reduced cortical thickness in abstinent alcoholics and association with alcoholic behavior. Alcohol Clin Exp Res.2011;35(12):2193–2201.

Fortier CB, Leritz EC, Salat DH, Lindemer E, Maksimovskiy AL, Shepel J, Williams V, Venne JR, Milberg WP, McGlinchey RE. Widespread effects of alcohol on white matter microstructure. Alcohol Clin Exp Res. 2014;38(12):2925-33.

Gazdzinski S, Durazzo TC, Mon A, Yeh PH, Meyerhoff DJ. Cerebral white matter recovery in abstinent alcoholics--a multimodality magnetic resonance study. Brain. 2010;133(Pt 4):1043-53.

Gilpin NW, Richardson HN, Cole M, Koob GF. Vapor inhalation of alcohol in rats. Curr Protoc Neurosci. 2008;Chapter 9:Unit 9.29.

Grant BF, Chou SP, Saha TD, Pickering RP, Kerridge BT, Ruan WJ, Huang B, Jung J, Zhang H, Fan A, Hasin DS. Prevalence of 12-Month Alcohol Use, High-Risk Drinking, and DSM-IV Alcohol Use Disorder in the United States, 2001-2002 to 2012-2013Results From the National Epidemiologic Survey on Alcohol and Related Conditions. *JAMA Psychiatry.* 2017;74(9):911–923.

Griffin WC. Alcohol dependence and free-choice drinking in mice. Alcohol. 2014; 48(3):287-93.

Griffin WC, Lopez MF, Yanke AB, Middaugh LD, Becker HC. Repeated cycles of chronic intermittent ethanol exposure in mice increases voluntary ethanol drinking and ethanol concentrations in the nucleus accumbens. Psychopharmacology (Berl). 2009;201(4):569-80.

Harper C. The neurotoxicity of alcohol. Hum Exp Toxicol. 2007;26(3):251-7.

Kim A, Zamora-martinez ER, Edwards S, Mandyam CD. Structural reorganization of pyramidal neurons in the medial prefrontal cortex of alcohol dependent rats is associated with altered glial plasticity. Brain Struct Funct. 2015;220(3):1705-20.

Kim JH, Budde MD, Liang HF, Klein RS, Russell JH, Cross AH, Song SK. Detecting axon damage in spinal cord from a mouse model of multiple sclerosis. Neurobiol Dis. 2006;21(3):626-32.

Konrad A, Vucurevic G, Lorscheider M, Bernow M, Thummel M, Chai C, Pfeifer P, Stoeter P, Scheurich A, Fehr C. Broad disruption of brain white matter microstructure and relationship with neuropsychological performance in male patients with severe alcohol dependence. Alcohol Alcohol. 2012;47(2):118-26.

Lewohl JM, Wixey J, Harper CG, Dodd PR. Expression of MBP, PLP, MAG, CNP, and GFAP in the Human Alcoholic Brain. Alcohol Clin Exp Res. 2005;29(9):1698-705.

Lewohl JM, Wang L, Miles MF, Zhang L, Dodd PR, Harris RA. Gene expression in human alcoholism: microarray analysis of frontal cortex. Alcohol Clin Exp Res. 2000;24(12):1873-82.

Ligon KL, Kesari S, Kitada M, Sun T, Arnett HA, Alberta JA, Anderson DJ, Stiles CD, Rowitch DH. Development of NG2 neural progenitor cells requires Olig gene function. Proc Natl Acad Sci USA. 2006; 103:7853-7858.

Lopez MF, Becker HC. Effect of pattern and number of chronic ethanol exposures on subsequent voluntary ethanol intake in C57BL/6J mice. Psychopharmacology (Berl). 2005; 181(4):688-96.

Lopez MF, Griffin WC, Melendez RI, Becker HC. Repeated cycles of chronic intermittent ethanol exposure leads to the development of tolerance to aversive effects of ethanol in C57BL/6J mice. Alcohol Clin Exp Res. 2012; 36(7):1180-7.

Macdonald CL, Dikranian K, Song SK, Bayly PV, Holtzman DM, Brody DL. Detection of traumatic axonal injury with diffusion tensor imaging in a mouse model of traumatic brain injury. Exp Neurol. 2007; 205(1):116-31.

Mandyam CD, Koob GF. The addicted brain craves new neurons: putative role for adult-born progenitors in promoting recovery. Trends Neurosci. 2012;35(4):250-60.

Mayfield RD, Lewohl JM, Dodd PR, Herlihy A, Liu J, Harris RA. Patterns of gene expression are altered in the frontal and motor cortices of human alcoholics. J Neurochem. 2002;81(4):802-13.

Mcbride WJ, Li TK. Animal models of alcoholism: neurobiology of high alcohol-drinking behavior in rodents. Crit Rev Neurobiol. 1998;12(4):339-69.

Mccormick LM, Ziebell S, Nopoulos P, Cassell M, Andreasen NC, Brumm M. Anterior cingulate cortex: an MRI-based parcellation method. Neuroimage. 2006;32(3):1167-75.

Mckenna BS, Brown GG, Archibald S, Scadeng M, Bussell R, Kesby JP, Markou A, Soontornniyomkjj V, Achim C, Semenova S. Microstructural changes to the brain of mice after methamphetamine exposure as identified with diffusion tensor imaging. Psychiatry Res. 2016;249:27-37.

Miguel-hidalgo JJ, Overholser JC, Meltzer HY, Stockmeier CA, Rajkowska G. Reduced glial and neuronal packing density in the orbitofrontal cortex in alcohol dependence and its relationship with suicide and duration of alcohol dependence. Alcohol Clin Exp Res. 2006;30(11):1845-55.

Montesinos J, Alfonso-loeches S, Guerri C. Impact of the Innate Immune Response in the Actions of Ethanol on the Central Nervous System. Alcohol Clin Exp Res. 2016;40(11):2260-2270.

Moorman DE, Aston-jones G. Prefrontal neurons encode context-based response execution and inhibition in reward seeking and extinction. Proc Natl Acad Sci USA. 2015;112(30):9472-7.

Moos RH, Moos BS. Rates and predictors of relapse after natural and treated remission from alcohol use disorders. Addiction. 2006;101(2):212-22.

Navarro AI, Mandyam CD. Protracted abstinence from chronic ethanol exposure alters the structure of neurons and expression of oligodendrocytes and myelin in the medial prefrontal cortex. Neuroscience. 2015;293:35-44.

O'Donnell LJ, Westin CF. An introduction to diffusion tensor image analysis. Neurosurg Clin N Am. 2011; 22(2):185-96, viii.

Oguz I, Mcmurray MS, Styner M, Johns JM. The translational role of diffusion tensor image analysis in animal models of developmental pathologies. Dev Neurosci. 2012;34(1):5-19.

Paxinos G, Watson C. The Rat Brain in Stereotaxic Coordinates. Academic Press;2009.

Pierpaoli C, Barnett A, Pajevic S, Chen R, Penix L, Virta A, Basser P. Water diffusion changes in Wallerian degeneration and their dependence on white matter architecture. NeuroImage. 2001;13: 1174–1185.

Pleil KE, Lowery-Gionta EG, Crowley NA, Li C, Marcinkiewcz CA, Rose JH, McCall NM, Maldonado-Devincci AM, Morrow AL, Jones SR, Kash TL. Effects of

chronic ethanol exposure on neuronal function in the prefrontal cortex and extended amygdala. Neuropharmacology. 2015;99:735-49.

Pfefferbaum A, Sullivan EV. Disruption of brain white matter microstructure by excessive intracellular and extracellular fluid in alcoholism: evidence from diffusion tensor imaging. Neuropsychopharmacology. 2005;30(2):423-32.

Pfefferbaum A, Adalsteinsson E, Sullivan EV. Dysmorphology and microstructural degradation of the corpus callosum: Interaction of age and alcoholism. Neurobiol Aging. 2006;27(7):994-1009.

Pfefferbaum A, Sullivan EV, Hedehus M, Adalsteinsson E, Lim KO, Moseley M. In vivo detection and functional correlates of white matter microstructural disruption in chronic alcoholism. Alcohol Clin Exp Res. 2000;24(8):1214-21.

Pfefferbaum A, Rosenbloom MJ, Chu W, Sassoon SA, Rohlfing T, Pohl KM, Zahr NM, Sullivan EV. White matter microstructural recovery with abstinence and decline with relapse in alcohol dependence interacts with normal ageing: a controlled longitudinal DTI study. Lancet Psychiatry. 2014;1(3):202-12.

Preston AR, Eichenbaum H. Interplay of hippocampus and prefrontal cortex in memory. Curr Biol. 2013;23(17):R764-73.

Privratsky JR, Newman PJ. PECAM-1: regulator of endothelial junctional integrity. Cell Tissue Res. 2014;355(3):607-19.

Richardson HN, Chan SH, Crawford EF, Lee YK, Funk CK, Koob GF, Mandyam CD. Permanent impairment of birth and survival of cortical and hippocampal proliferating cells following excessive drinking during alcohol dependence. Neurobiol Dis. 2009;36(1):1-10.

Rivers LE, Young KM, Rizzi M, Jamen F, Psachoulia K, Wade A, Kessaris N, Richardson WD. PDGFRA/NG2 glia generate myelinating oligodendrocytes and piriform projection neurons in adult mice. Nat Neurosci. 2008;11:1392–1401.

Robinson G, Most D, Ferguson LB, Mayfield J, Harris RA, Blednov YA. Neuroimmune pathways in alcohol consumption: evidence from behavioral and genetic studies in rodents and humans. Int Rev Neurobiol. 2014;118:13-39.

Rosenbloom M, Sullivan EV, Pfefferbaum A. Using magnetic resonance imaging and diffusion tensor imaging to assess brain damage in alcoholics. Alcohol Res Health. 2003;27(2):146-52.

Rosenbloom MJ, Pfefferbaum A. Magnetic resonance imaging of the living brain: evidence for brain degeneration among alcoholics and recovery with abstinence. Alcohol Res Health. 2008;31(4):362-76.

Samantaray S, Knaryan VH, Patel KS, Mulholland PJ, Becker HC, Banik NL. Chronic intermittent ethanol induced axon and myelin degeneration is attenuated by calpain inhibition. Brain Res. 2015;1622:7-21.

Substance Abuse and Mental Health Services Administration (SAMHSA). National Survey on Drug Use and Health (NSDUH). Table 5.6A—Substance Use Disorder in Past Year among Persons Aged 18 or Older, by Demographic Characteristics: Numbers in Thousands, 2014 and 2015. 2015.

Schulteis G, Hyytiä P, Heinrichs SC, Koob GF. Effects of chronic ethanol exposure on oral self-administration of ethanol or saccharin by Wistar rats. Alcohol Clin Exp Res. 1996;20(1):164-71.

Smith ML, Lopez MF, Archer KJ, Wolen AR, Becker HC, Miles MF. Time-Course Analysis of Brain Regional Expression Network Responses to Chronic Intermittent Ethanol and Withdrawal: Implications for Mechanisms Underlying Excessive Ethanol Consumption. PLoS ONE. 2016;11(1):e0146257.

Soares JM, Marques P, Alves V, Sousa N. A hitchhiker's guide to diffusion tensor imaging. Front Neurosci. 2013;7:31.

Somkuwar SS, Staples MC, Galinato MH, Fannon MJ, Mandyam CD. Role of NG2 expressing cells in addiction: a new approach for an old problem. Front Pharmacol. 2014;5:279.

Somkuwar SS, Fannon MJ, Staples MC, Zamora-Martinez ER, Navarro AI, Kim A, Quigley JA, Edwards S, Mandyam CD. Alcohol dependence-induced regulation of the proliferation and survival of adult brain progenitors is associated with altered BDNF-TrkB signaling. Brain Struct Funct. 2015;221(9):4319-4335.

Somkuwar SS, Fannon-Pavlich MJ, Ghofranian A, Quigley JA, Dutta RR, Galinato MH, Mandyam CD. Wheel running reduces ethanol seeking by increasing neuronal activation and reducing oligodendroglial/neuroinflammatory factors in the medial prefrontal cortex. Brain Behav Immun. 2016;58:357-368.

Song SK, Sun SW, Ramsbottom MJ, Chang C, Russell J, Cross AH. Dysmyelination revealed through MRI as increased radial (but unchanged axial) diffusion of water. Neuroimage. 2002;17(3):1429-36.

Song SK, Yoshino J, Le TQ, Lin SJ, Sun SW, Cross AH, Armstrong RC. Demyelination increases radial diffusivity in corpus callosum of mouse brain. Neuroimage. 2005;26(1):132-40.

Sorg SF, Taylor MJ, Alhassoon OM, Gongvatana A, Theilmann RJ, Frank LR, Grant I. Frontal white matter integrity predictors of adult alcohol treatment outcome. Biol Psychiatry. 2012;71(3):262-8.

Sun Y, Meijer DH, Alberta JA, Mehta S, Kane MF, Tien AC, Fu H, Petryniak MA, Potter GB, Liu Z, Powers JF, Runquist IS, Rowitch DH, Stiles CD. Phosphorylation state of Olig2 regulates proliferation of neural progenitors. Neuron. 2011;69:906–917.

Valdez GR, Roberts AJ, Chan K, Davis H, Brennan M, Zorrilla EP, Koob GF. Increased ethanol self-administration and anxiety-like behavior during acute ethanol withdrawal and abstinence: regulation by corticotropin-releasing factor. Alcohol Clin Exp Res. 2002;26(10):1494-501.

Valles SL, Blanco AM, Pascual M, Guerri C. Chronic ethanol treatment enhances inflammatory mediators and cell death in the brain and in astrocytes. Brain Pathol. 2004;14:365–371.

Van Skike CE, Diaz-granados JL, Matthews DB. Chronic intermittent ethanol exposure produces persistent anxiety in adolescent and adult rats. Alcohol Clin Exp Res. 2015;39(2):262-71.

Vetreno RP, Hall JM, Savage LM. Alcohol-related amnesia and dementia: Animal models have revealed the contributions of different etiological factors on neuropathology, neurochemical dysfunction and cognitive impairment. Neurobiology of learning and memory. 2011;96(4):596-608.

Weilbächer RA, Gluth S. The Interplay of Hippocampus and Ventromedial Prefrontal Cortex in Memory-Based Decision Making. Brain Sci. 2016;7(1):4.

Whitman BA, Knapp DJ, Werner DF, Crews FT, Breese GR. The cytokine mRNA increase induced by withdrawal from chronic ethanol in the sterile environment of brain is mediated by CRF and HMGB1 release. Alcohol Clin Exp Res. 2013;37(12):2086-97.

Wolf OT, Dyakin V, Vadasz C, De leon MJ, Mcewen BS, Bulloch K. Volumetric measurement of the hippocampus, the anterior cingulate cortex, and the retrosplenial granular cortex of the rat using structural MRI. Brain Res Brain Res Protoc. 2002;10(1):41-6.

Woodfin, A., Voisin, M.B., Nourshargh, S., 2007. PECAM-1: a multi-functional molecule in inflammation and vascular biology. Arterioscler. Thromb. Vasc. Biol. 2008;27: 2514–2523.

Wu QZ, Yang Q, Cate HS, Kemper D, Binder M, Wang HX, Fang K, Quick MJ, Marriott M, Kilpatric TJ, Egan GF. MRI identification of the rostral-caudal pattern of pathology within the corpus callosum in the cuprizone mouse model. J Magn Reson Imaging. 2008;27(3):446-53.

Zahr NM, Pfefferbaum A. Alcohol's Effects on the Brain: Neuroimaging Results in Humans and Animal Models. Alcohol Research: Current Reviews. 2017;38(2):183-206.

Zahr NM, Sullivan EV. Translational studies of alcoholism: bridging the gap. Alcohol Res Health. 2008;31(3):215-30.

Zhang J, Jones MV, Mcmahon MT, Mori S, Calabresi PA. In vivo and ex vivo diffusion tensor imaging of cuprizone-induced demyelination in the mouse corpus callosum. Magn Reson Med. 2012;67(3):750-9.

Zou Y, Murray DE, Durazzo TC, Schmidt TP, Murray TA, Meyerhoff DJ. Effects of abstinence and chronic cigarette smoking on white matter microstructure in alcohol dependence: Diffusion tensor imaging at 4T. Drug Alcohol Depend. 2017;175:42-50.